Continuous-wave second harmonic generation in Bragg reflection waveguides

Payam Abolghasem, Junbo Han, Bhavin J. Bijlani, Arghavan Arjmand and Amr S. Helmy

The Edward S. Rogers Sr. Department of Electrical and Computer Engineering, University of Toronto, 10 King's College Road, Toronto, Ontario M5S 3G4, Canada

a.helmy@utoronto.ca

http://photonics.light.utoronto.ca/helmy/

Abstract: We report the observation of continuous-wave second harmonic generation for a pump at 1559.9 nm in type-I phase-matched Bragg reflection waveguide using the GaAs/$Al_xGa_{1-x}As$ material system. For an internal pump power of 94 mW, phase-matched second harmonic power of 23 nW was measured in a waveguide with a length of 1.96 mm and ridge width of 4 μm. The internal conversion efficiency of the process was estimated as 6.8×10^{-3} $\%W^{-1}cm^{-2}$. The full-width at half-maximum bandwidth of the nonlinear process was found to be 0.91 nm.

OCIS codes: (190.2620) Harmonic generation and mixing; (190.4390) Nonlinear optics, integrated optics.

References and links

1. P. S. Kuo, K. L. Vodopyanov, M. M. Fejer, X. Yu, J. S. Harris, D. F. Bliss, and D. Weyburne, "GaAs optical parametric oscillator with circularly polarized and depolarized pump," Opt. Lett. **32**, 2735–2737 (2007).
2. S. Tanzilli, H. De Riedmatten, W. Tittel, H. Zbinden, P. Baldi, M. De Micheli, D. .B. Ostrowsky, and N. Gisin, "Highly efficient photon-pair source using periodically poled lithium niobate waveguide," Ellectron. Lett. **37**, 26–28 (2001).
3. A. S. Helmy, "Phase matching using Bragg reflection waveguides for monolithic nonlinear optics applications," Opt. Express **14**, 1243–1252 (2006).
4. A. S. Helmy, B. Bijlani and P. Abolghasem, "Phase matching in monolithic Bragg reflection waveguides," Opt. Lett. **32**, 2399–2401 (2007).
5. B. Bijlani, P. Abolghasem, and A. S. Helmy, "Second harmonic generation in ridge Bragg reflection waveguides," Appl. Phys. Lett. **92**, 101124 (2008).
6. A. S. Helmy, D. C. Hutchings, T. C. Kleckner, J. H. Marsh, A. C. Bryce, J. M. Arnold, C. R. Stanley, J. S. Aitchison, C. T. A. Brown, K. Moutzouris, and M. Ebrahimzadeh, "Quasi phase matching in GaAs-AlAs superlattice waveguides through bandgap tuning by use of quantum-well intermixing," Opt. Lett. **25**, 1370–1372 (2000).
7. A. Fiore, S. Janz, L. Delobel, P. van der Meer, P. Bravetti, V. Berger, and E. Rosencher, "Second-harmonic generation at $\lambda = 1.6$ μm in AlGaAs/Al_2O_3 waveguides using birefringence phase matching," Appl. Phys. Lett. **72**, 2942–2944 (1998).
8. R. Haidar, N. Forget, and E. Rosencher, "Optical parametric oscillation in microcavities based on isotropic semiconductors: A theoretical. study," IEEE J. Quantum Electron. **39**, 569–576 (2003).
9. Y. Shih, "Entangled biphoton source-property and preparation," Rep. Prog. Phys. **66**, 1009–1044 (2003).
10. S. Sauge, M. Swillo, S. Alber-Seifried, G. B. Xavier, J. Waldeback, M. Tengner, D. Ljunggren, and A. Karlesson, "Narrowband polarization-entangled photon pairs distributed over a WDM link for qubit networks," Opt. Express **15**, 6926–6933 (2007).

#109604 - $15.00 USD Received 3 Apr 2009; revised 13 May 2009; accepted 16 May 2009; published 21 May 2009

11. K. Moutzouris, S. V. Rao, M. Ebrahimzadeh, A. De Rossi, M. Calligaro, V. Ortiz and Berger V, " Second-harmonic generation through optimized modal phase matching in semiconductor waveguides," Appl. Phys. Lett. **83**, 620–622 (2003).
12. T. Feuchter and C. Thristrup, "High-precision planar wave-guide propagation loss measurement technique using a Fabry-Perot cavity," IEEE Photon. Tech. Lett. **6**, 1244–1247 (1994).
13. B. R. West and A. S. Helmy, "Analysis and design equations for phase matching using Bragg reflector waveguides," IEEE J. Quantum Electron. **12**, 431–442 (2006).
14. A. De Rossi, V. Ortiz, M. Calligaro, L. Lanco, S. Ducci, V. Berger and I. Sagnes, "Measuring propagation loss in a multimode semiconductor waveguide," Appl. Phys. Lett. **97**, 073105 (2005).
15. M. M. Fejer, G. A. Magel, D. H. Jundt, and R. L. Byer, "Quasi-phase-matched 2nd harmonic-generation - tuning and tolerances," IEEE J. Quantum Electron. **28**, 2631–2654 (1992).
16. S. Gehrsitz, F. K. Reinhart, C. Gourgon, N. Herres, A. Vonlanthen and H. Sigg, "The refractive index of Al_xGa1_xAs below the band gap: Accurate determination and empirical modeling," Appl. Phys. **87**, 7825–7837 (2000).
17. J. Talghader, J. S. Smith, "Thermal dependence of the refractive index of GaAs and AlAs measured using semiconductor multilayer optical cavities," Appl. Phys. Lett. **69**, 2608–2608 (1996).
18. M. L. Bortz, S. J. Field, M. M. Fejer, D. W. Nam, R. G. Waarts, and D. F. Welch, "Noncritical quasi-phase-matched 2nd-harmonic generation in an annealed proton-exchanged $LiNbO_3$ waveguide," IEEE J. Quantum Electron. **30**, 2953–2960 (1994).
19. S. J. Wagner, A.A. Muhairi, J. S. Aitchison, and A. S. Helmy, "Modeling and optimization of quasi-phase matching via domain-disordering," IEEE J. Quantum Electron. **44**, 424–429 (2008).
20. B. Monemar, K. K. Shih, and G. D. Pettit, "Some optical properties of the $Al_xGa_{1-x}As$ alloys system," Appl. Phys. **47**, 2604–2613 (1976).

1. Introduction

Integrated parametric devices harnessing second order nonlinearities in III-V semiconductors have attracted increasing attention in recent years. Examples of monolithically integrated devices that utilize second order nonlinearities could include optical parametric oscillators (OPOs), frequency conversion elements and integrated entangled photon-pair sources [1]. The increasing demand for robust, tunable and cost effective integrated OPOs renders the practical realization of monolithic versions of such sources essential. Another class of devices with emerging significance is a source for photon-pairs, which is an essential ingredient for quantum information processing systems [2]. The performance of integrated parametric devices chiefly relies on the phase-matching (PM) scheme which harnesses the nonlinearities.

Recently, we have proposed a phase-matching technique using Bragg reflection waveguides (BRWs) [3] in monolithic $Al_xGa_{1-x}As$ waveguides and successfully demonstrated its performance in a device for second-harmonic generation (SHG) [4, 5]. BRWs are particularly attractive as their structure is similar to the vertical-cavity surface-emitting lasers (VCSELs). Unlike other phase-matching techniques such as quasi-phase matching (QPM) [6], form birefringence [7] and high Q-resonant cavities [8] which involve over growth on $Al_xGa_{1-x}As$ elements or growth on oxide layers, BRW phase-matching benefit from easier fabrication techniques making them more amenable for monolithically integration with diode pump lasers. While previously reported SHG in BRWs used picosecond pulses [4, 5], continuous-wave (CW) characterization of these devices has yet to be addressed.

In this work, we report the performance of CW-SHG using phase-matched BRW. The operation of these structures in the CW regime is important, particularly for quantum information processing applications, where efficient photon-pair sources based on spontaneous parametric down conversion (SPDC) can be realized. CW operation is particularly essential for generating twin photons with maximally entangled properties [9]. Also, in a quantum communication link, photon-pairs with narrow bandwidth are indispensable for increasing the transmission distance by means of reducing chromatic dispersion effects [10]. The technique used in this work for PM is attractive in that it offers unparalleled control over several linear and nonlinear attributes of the device, while maintaining PM in a monolithic setting.

#109604 - $15.00 USD Received 3 Apr 2009; revised 13 May 2009; accepted 16 May 2009; published 21 May 2009

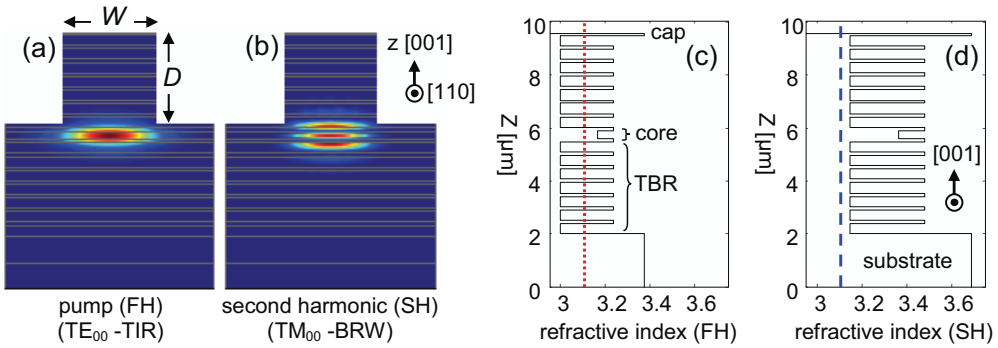

Fig. 1. Schematic of a ridge BRW with ridge width W and etch depth D superimposed by simulated (a) intensity profile of TE-polarized pump (FH) and (b) intensity profile of TM-polarized second harmonic. (c) Index profile at FH frequency and (d) index profile at SH frequency obtained using the model in [16]. The red dotted line in (c) is the effective mode index of the FH and the blue dashed line in (d) is that of the SH. The samples fabricated had W varying between 2.5 μm-4.5 μm and $D \approx 3.4$ μm.

2. Device description and fabrication

Phase-matching using Bragg reflection waveguides is an exact phase-matching technique rely on modal dispersion properties of the interacting frequencies [3]. In this scheme, for SHG the pump signal (FH) propagates as a conventional total internal reflection mode (TIR) while the propagation of the second-harmonic (SH) is supported through reflections from the transverse Bragg reflectors (TBRs). Unlike other modal phase-matching techniques in $Al_xGa_{1-x}As$ [11] where PM is obtained between high order modes, BRW phase-matching attains PM between the lowest order modes of pump and second-harmonic. This allows maximum utilization of the powers of both harmonics for the nonlinear interaction.

A representative ridge BRW along with typical intensity profiles of the pump and frequency doubled signal is illustrated in Fig. 1. The wafer used was grown on a GaAs [001] substrate using metal-organic chemical vapour deposition (MOCVD). The top and bottom transverse Bragg reflectors (TBRs) consisted of 7 periods of bi-layers $Al_{0.25}Ga_{0.75}As/Al_{0.75}Ga_{0.25}As$ with thicknesses 123 nm/391 nm, respectively. The $Al_{0.40}Ga_{0.60}As$ core had a thickness of 300 nm. The sample was capped with a 50 nm layer of GaAs. Waveguide ridges with widths 2.5 μm-4.5 μm with 0.5 μm steps were patterned through plasma etching for a depth of ≈ 3.4 μm. The cleave plane was normal to the [110] direction to access nonzero elements of the χ^2 tensor. The length of the sample was 1.96 mm. Detailed characterization of the waveguide with 4 μm ridge width is discussed in the next section.

3. Characterization results

Characterization of the waveguide linear properties was carried out using the Fabry-Pèrot method [12] utilizing a single-mode tuneable laser source at low power (≈ 2 mW) in the wavelength range around 1560 nm. For TE-polarization, linear propagation loss (α_ω) of 7.78 cm^{-1}, input coupling efficiency (C) of 50% and facet reflectivity (R) of 29%, were the typical values measured. During the design it was attempted to design the devices with linear loss values less than 1.0 cm^{-1} by undertaking several steps including: (1) selecting aluminum concentrations more than 0.24 ($x > 0.24$) to reduce material absorption by shifting the materials bandgap away from the operating wavelength and (2) curtailing transverse leakage losses by using TBRs with high refractive index contrast bi-layers. However, in comparison to previously character-

#109604 - $15.00 USD Received 3 Apr 2009; revised 13 May 2009; accepted 16 May 2009; published 21 May 2009

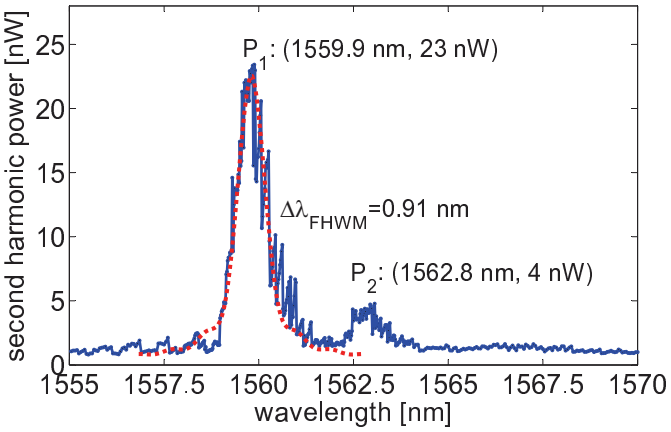

Fig. 2. Second harmonic power ($P_{2\omega}$) vs. tuning of fundamental wavelength. Solid line is the experimental data and the dotted line is a theoretical tuning curve obtained using beam propagation method. The theoretical curve is simulated by including the propagation loss of FH and an estimated loss of SH to match the full-width at half-maximum bandwidths of the two curves.

ized phase-matched BRWs [4, 5], the current design denotes increased propagation losses. We mainly attribute the large measured propagation loss to the plasma etch quality. It is worth mentioning that the choice of $x > 0.24$ in $Al_xGa_{1-x}As$ layers for loss reduction was expected to degrade the nonlinear interaction by reducing the effective χ^2 value. This effect was partly tackled by improving the nonlinear overlap factor between the harmonics [13]. Detail design optimization is required to fully address this trade-off.

Also, it can be seen that the measured value of 50% for the input coupling efficiency was higher than what is routinely reported in similar structures. Accurate estimation of the coupling efficiency in the BRW was problematic due to the fact that linear characterization based on Fabry-Pèrot method provides good results when the device under test supports single mode propagation [14]. This is not valid for the characterized device where multi-modedness exists in both lateral and transverse directions. To get a better insight of the input coupling factor, we simulated this parameter by calculating the overlap integral between the field profiles of the pump beam and the excited fundamental mode. The simulation resulted in an overlap factor of 54%. Comparing the experimentally measured coupling factor with the simulated value, we find 7% error in the measured value of the input coupling efficiency.

It is worth mentioning that although the characterized waveguide supports multi-mode propagation, we claim that the Fabry-Pèrot method provided an accurate estimation of the linear loss value as the linear transmission spectrum of the device illustrated clear Fabry-Pèrot fringes at the wavelength range of interest. Despite the fact that higher order modes were excited at the input facet of the waveguide, they were filtered out from the detected output signal through loss discrimination mechanism.

The characterization of the nonlinear properties was carried out using the same setup discussed above. Using a C-band Erbium-doped fiber-amplifier (EDFA), the pump power was amplified to ≈ 265 mW, which was measured before the front facet of the device. Taking into account 29% facet reflectivity and 50% end-fire coupling efficiency, one obtains internal FH power of $P_\omega \approx 94$ mW at the input facet. Second harmonic power was then monitored using a Germanium photo detector over the relevant wavelength range to obtain the tuning curve. Internal SH power ($P_{2\omega}$), estimated right before the output facet, was obtained by accounting for

#109604 - $15.00 USD Received 3 Apr 2009; revised 13 May 2009; accepted 16 May 2009; published 21 May 2009

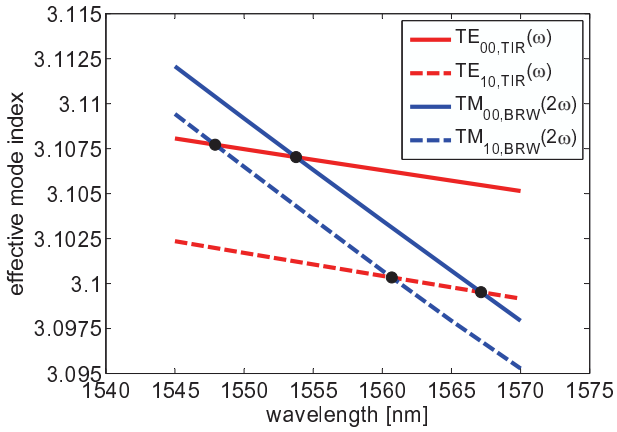

Fig. 3. Calculations of the phase-matching conditions between higher order modes of the FH and SH. The filled circles where two curves cross indicate wavelengths for which type-I phase-matching condition is satisfied. A discrepancy of ≈ 6 nm exists between the experimental phase-matching wavelength at 1559.9 nm in Fig. 2 and the simulated value where the curves of $\mathrm{TE}_{00}(\omega)$ and $\mathrm{TM}_{00}(2\omega)$ crosses.

the transmission of the output objective lens (57%) and the facet reflectivity (29%). Figure 2 illustrates the resulted tuning curve in terms of the internal SH power. As can be observed in the Fig. 2, the peak SH power of 23 nW is evident at the phase-matching wavelength (λ_{PM}) of 1559.9 nm. The structure was designed for PM to take place at 1550 nm for the slab case, without taking into account ridge effects. However, red-shift of λ_{PM} was anticipated as a result of the lateral confinement imposed by the ridge structure.

The tuning curve illustrated in Fig. 2 indicates an additional SH resonance (P_2) at 1562.8 nm. This extra peak does not resemble the side lobe of a sinc^2 function [15] and hence merits further attention. Initially, the experimental tuning curve was compared with a theoretical one in the ideal case, where the linear/nonlinear losses were ignored. It is well known that for a sample of length L, $P_{2\omega} \propto \mathrm{sinc}^2(\Delta kL/2)$, where $\Delta k = k(2\omega) - 2k(\omega)$ is the phase mismatch. From the theoretical tuning curve, the separation between the peak of the main lobe of the sinc^2 function and the immediate side lobes was found to be ≈ 1.0 nm. However, the feature at $\lambda_{\mathrm{P}_2} = 1562.8$ nm lies 2.9 nm away from the phase-matching point at 1559.9 nm, in contrast to the ideal case of 1.0 nm. We further investigated the possibility of having phase-matching among higher order modes of FH and SH. The simulations indicated modal phase-matching between higher order modes could indeed exist. For example, as illustrated in Fig. 3, phase-matching condition can be satisfied between $\mathrm{TE}_{00,\mathrm{TIR}}(\omega)$ and $\mathrm{TM}_{10,\mathrm{BRW}}(2\omega)$ with the peak SH power 5.8 nm below λ_{P_1}. Also $\mathrm{TE}_{10,\mathrm{TIR}}(\omega)$ and $\mathrm{TM}_{10,\mathrm{BRW}}(2\omega)$ can be phase-matched at 6.9 nm above λ_{P_1}. Phase-matching between $\mathrm{TE}_{10,\mathrm{TIR}}(\omega)$ and $\mathrm{TM}_{10,\mathrm{BRW}}(2\omega)$ is more likely accountable for the SH feature at λ_{P_2}. Discrepancies between the calculated predictions and measurements could be due to fabrication tolerances. To investigate the multimoded nature of the waveguide, we studied the Fabry-Pèrot fringes of FH at high pump power. In Fig. 4-a and -b, we have compared the FH transmittance at low pump power of 2 mW used for linear loss measurement and the FH transmittance at high power of 265 mW used for second-harmonic generation, respectively. As can be seen from Fig. 4-a, the uniform Fabry-Pèrot fringes is a strong evidence of single mode propagation when 2 mW pump is launched in the waveguide. In contrast, the Fabry-Pèrot fringes in Fig. 4-b exhibit a behaviour characteristic of multimode waveguides. The multimode behaviour at high pump power can be ascribed to two effects.

#109604 - $15.00 USD Received 3 Apr 2009; revised 13 May 2009; accepted 16 May 2009; published 21 May 2009

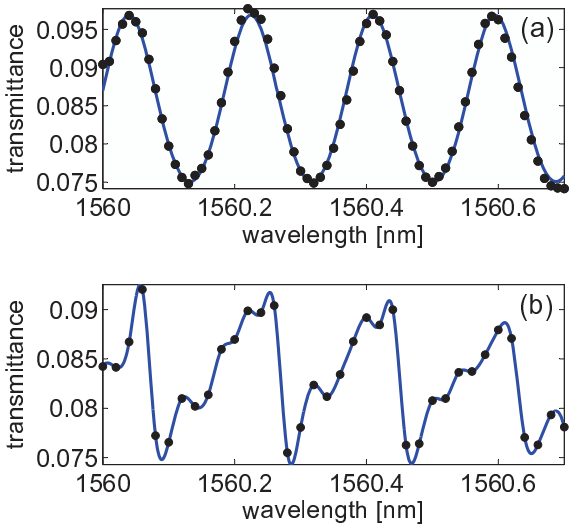

Fig. 4. Transmittance of pump vs. wavelength at (a) input power level of 2 mW used for linear characterization and (b) input power level of 265 mW used for SHG experiment. In both Figs. circles are the measured data. The solid line in (a) is the fit to the Airy's transmission of the pump and that in (b) is obtained using an interpolating fit. The non-uniform transmittance spectrum in (b) clearly denotes the effect of high order modes superposition in the detected signal at high input pump power.

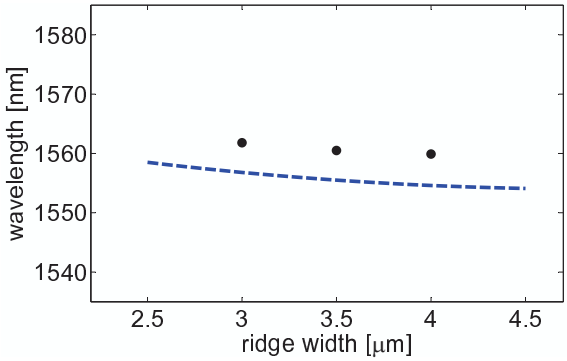

Fig. 5. Variation of phase matching wavelength as a function of the ridge width. The points are the experimentally measured data, while the dashed line is obtained from simulation.

First, higher order modes contain more power at higher pump and hence can contribute to the nonlinear conversion with output powers above the detection limit. Second, increasing the pump power results in an increase of the core temperature where power confinement is the highest. This, in turn, increases the core refractive index [16, 17]. As a result, the waveguide acquires an enhanced index difference between the core and the lateral claddings, making it more multimoded.

We further characterized waveguides with ridge widths of 3 μm and 3.5 μm for the linear/nonlinear parameters of interest. Fig. 5 shows the phase-matching wavelength shift as a function of ridge width obtained experimentally and its comparison with those obtained numerically. Both methods predict the red-shift of phase-matching wavelength with decreasing

#109604 - $15.00 USD Received 3 Apr 2009; revised 13 May 2009; accepted 16 May 2009; published 21 May 2009

ridge size. The difference between the experimental and measured values of λ_{PM} were less than 6 nm for all three devices. It should be notice that the characterized BRWs were composed of 30 layers of $Al_xGa_{1-x}As$ elements. Tolerances in growing the structure, inaccuracies in refractive index model and material dispersion [16], as well as roughness in patterning the waveguides due to the dry etching process, could all contribute to deviation between theoretical and experimental predictions. Given the uncertainties involved, we believe that the reported 6 nm mismatch between theoretical and experimental values of phase-matching wavelength is an acceptable disagreement between the two models.

The internal nonlinear conversion efficiency of the process, taken as $\eta = P_{2\omega}/P_{\omega}^2$, was estimated to be $\approx 2.7 \times 10^{-4}$ $\%W^{-1}$. A figure of merit which indicates the performance of the SHG device and is independent of the waveguide length is the normalized conversion efficiency defined as $\eta_{norm} = \eta/L^2$, where $L = 1.96$ mm is the waveguide length. Here, we obtained $\eta_{norm} \approx 6.8 \times 10^{-3}$ $\%W^{-1}cm^{-2}$. It would be instructive to compare the CW conversion efficiency in our device with that obtained in a pulsed laser setup. We characterized the waveguide using a mode-locked Ti:Sapphire pumped OPO. The employed pulses were nearly transform-limited with a temporal width of ≈ 2.5 ps and a repetition rate of 76 MHz. For a FH average power of 115 mW (41 mW inside the waveguide), peak SH power of 2.4 μW was measured at the phase-matching wavelength of $\lambda = 1559.7$ nm. The normalized conversion efficiency of the process was then estimated to be $\eta_{norm} \approx 3.7$ $\%W^{-1}cm^{-2}$, indicating over 2.7 orders of magnitude increase compare to the efficiency of the CW case. This enhancement is attributed to significantly larger peak intensity in the pulsed regime in comparison to the CW one. For the FH mode with an effective mode area of 4.6 μm^2, the peak intensity of the coupled power inside the waveguide in the pulsed system was 4.5 GW/cm^2, while that in the CW experiment was 2.0 MW/cm^2. The ratio of the FH peak intensity in the pulse system was found to be ≈ 3.3 orders of magnitude larger than that in the CW experiment. This ratio is in the same order of magnitude of the ratio of the conversion efficiencies (≈ 2.7). The fact that the ratio of the peak intensities is larger than the ratio of the conversion efficiencies suggests the increased losses in the pulsed system which is accounted for by the two-photon absorption of the pump signal.

From the tuning curve of Fig. 2, the full-width at half-maximum (FWHM) bandwidth of the process was found to be ≈ 0.91 nm after filtering out the Fabry-Pèrot components of the FH from the spectrum. Ignoring harmonics losses, a theoretical estimation of the bandwidth can be obtained as [15]:

$$\Delta\lambda_{FWHM} = \frac{0.4429\lambda}{L}\left|\frac{\partial n_{eff}(\omega)}{\partial\lambda} - \frac{1}{2}\frac{\partial n_{eff}(2\omega)}{\partial\lambda}\right| \quad (1)$$

where λ is the FH wavelength and $n_{eff}(\omega)$ and $n_{eff}(2\omega)$ are, respectively, the effective modal indices of FH and SH. Here, we modelled $\Delta\lambda_{FWHM} = 0.78$ nm, indicating a factor of 1.16 difference between theoretical and the measured values. The increase in the process bandwidth suggests inhomogeneous broadening as a result of waveguide losses at interacting frequencies as well as fabrication imperfections [18]. Using beam propagation method [19] which includes harmonics losses, a SH loss value of 41 cm^{-1} was estimated by fitting the FWHM bandwidth of a normalized theoretical tuning curve to that of the experimental one (see dotted curve in Fig. 2). The estimated SH loss appeared to be larger than what was expected for this device. Several mechanisms can be accounted for this large loss value. First, in type-I PM where SH has TM polarization, substrate and cover leakage losses are more prominent as the direction of the electric field is dominantly normal to the interfaces formed by different layers. Second, the boundaries between adjacent layers can form rough interfaces which contribute to scattered losses. This source of loss is expected to be more significant in BRWs where the structure is composed of many dielectric layers. Finally, material absorption contributes to additional losses as the SH wavelength lies in proximity of the band-tail absorption of low aluminum

#109604 - $15.00 USD Received 3 Apr 2009; revised 13 May 2009; accepted 16 May 2009; published 21 May 2009

concentration layers [20]. It would be instructive to compare the estimated SH loss with linear loss of TM-polarized FH. Using Fabry-Pèrot technique, a loss value of 11.1 cm^{-1} was measured for TM-polarized FH around 1560 nm where PM was taking place. Taking into consideration the discussed sources of losses in BRWs, the estimated SH loss value of 41 cm^{-1} appears as a rough estimation in the characterized device.

4. Conclusion

In summary, we demonstrated CW-SHG using BRW design for frequency doubling of IR signals. For an internal FH power of 94 mW peak SH power of 23 nW was detected. The nonlinear conversion efficiency was estimated to be 6.8×10^{-3} $\%W^{-1}cm^{-2}$ with the process FHWM bandwidth of 0.91 nm. Linear loss of the device was measured to be 7.78 cm^{-1}. Using beam propagation method, SH loss was simulated to be 41 cm^{-1}. Using these results, we envision future integrated devices utilizing other parametric processes such as spontaneous parametric down-conversion, difference frequency generation and optical parametric oscillation.

Acknowledgments

The authors gratefully acknowledge the support of the Natural Sciences and Engineering Research Council of Canada (NSERC), Ontario Centres of Excellence (OCE) and CMC Microsystems.

#109604 - $15.00 USD Received 3 Apr 2009; revised 13 May 2009; accepted 16 May 2009; published 21 May 2009